Experimental study on the effect of pyrolysis pressure, peak temperature, and particle size on the potential stability of vine shoots-derived biochar

Joan J. Manyà,[*]*, Miguel A. Ortigosa, Sergio Laguarta, and José A. Manso*

Thermo-chemical Processes Group (GPT), Aragón Institute of Engineering Research (I3A), University of Zaragoza, Technological College of Huesca, crta. Cuarte s/n, E-22071, Huesca, Spain

[*] Corresponding author: Joan J. Manyà. E-mail address: joanjoma@unizar.es. Fax: +34 974239302.

HIGHLIGHTS

- A central composite design was applied to assessing the effect of pressure, peak temperature, and particle size on the potential stability-related properties of vine-shoots derived biochar.
- For the range of operating conditions used in this study, te potential stability of the vine shoots-derived biochar was mainly determined by the particle size. Pressure did not play any significant role.
- Using a bed of activated alumina particles represents a low-cost way to partly remove tar and simultaneously improve the product gas yield and composition.

ABSTRACT

This study examines the effect of three key operating factors (peak temperature, particle size and pressure) on the potential stability of the biochar produced by slow pyrolysis of vine shoots. The following response variables were considered as key indicators of the potential stability of biochar in soils: the fixed-carbon yield, the fraction of aromatic carbon, and the molar H:C and O:C ratios. Slow pyrolysis tests were conducted in a laboratory-scale fixed-bed unit and planned according to a 2-level factorial design. The behavior of the product gas yield and composition at the outlet of the secondary cracking reactor (a fixed-bed of activated alumina particles at 700 °C) was also evaluated as a function of the three factors. The results from the statistical tests revealed that the particle size is the most significant factor in determining the potential stability of biochars. Using larger particles of biomass and, in a lesser extent, operating at higher peak temperatures leads to the production of more stable materials. Unexpectedly, the absolute pressure only plays a significantly positive role in decreasing the tar content in the producer gas at the outlet of a secondary cracking reactor.

KEYWORDS

Biochar; Pyrolysis; Vine Shoots; Pressure; Peak Temperature; Particle Size; Aromatic C.

1. Introduction

Recently, increasing attention has been focused on biochar, because of its potential to simultaneously sequester carbon and amend agricultural soils [1-3]. Biochar is typically produced from the conventional carbonization or slow pyrolysis of biomass, because of the ability of this thermochemical process to yield more charcoal, at the expense of mainly the liquid fraction [4]. Although a large number of published studies have analyzed the effects of biochar addition to soils on the soil carbon cycle and plant growth, little attention has been directed toward determining the most appropriate process conditions to produce a charcoal suitable for the long-term storage of carbon [3,5].

It is well known that several operating parameters influence the behavior of the slow pyrolysis process. Among these, the peak temperature, the absolute pressure, and the particle size play an important role in determining both the biochar yield and the fixed-carbon content. The peak temperature is defined as the highest temperature reached during the pyrolysis process [6]. From the numerous experimental results available in the literature, it can be stated that, as a general rule, the biochar yield decreases as the peak temperature increases [7-11]. In contrast, increasing the peak temperature has a positive effect on the carbonization efficiency, enhancing the fixed-carbon yield [6,12-15]. In regard to the effect of the peak temperature on several properties of the biochar that are related to its potential application as a carbon sequestration and soil amendment agent, recent studies indicate that an increase in the peak temperature (generally from 400 to 600 °C) leads to an increase in the proportion of aromatic carbon [14,16-18]. Moreover, a decrease in both H:C and O:C molar ratios with rising the peak temperature has also been observed in earlier studies [13,18,19]. All of these findings reveal that an increase of the peak temperature could be a way to improve the chemical recalcitrance of the biochar, that is, its stability and resistance against biotic and abiotic oxidation.

Concerning the effect of the pressure on the pyrolysis behavior, previous investigations reported an increase of both the biochar yield and fixed-carbon content as the pressure was raised

from atmospheric to 0.5–3.0 MPa [20-22]. This finding is usually attributed to the enhancement of the secondary reactions, as a result of which additional charcoal is produced through the repolymerization of the volatile matter [6]. However, this enhancement can also be achieved simply by increasing the gas residence time inside the pyrolysis reactor [23]. In other words, the intrinsic effect of the pressure should be evaluated keeping constant the gas residence time (for example,). Regarding the influence of the pyrolysis pressure on the potential stability of the produced biochars, little information is given in the literature. Melligan and co-workers [24] observed, for biochars obtained by pyrolysis of miscanthus at a peak temperature of 550 °C, a progressive decrease in both the H:C and O:C molar ratios and a gradual increase in the proportion of aromatic C when the pressure was raised from atmospheric to 2.6 MPa in steps of 0.5 MPa. Hence, increasing the pressure could also be a convenient way to improve the potential stability of biochar.

In regard to the third factor, the particle size of the biomass feedstock, previous studies reported an increase in the charcoal yield as the particle size was increased [8,25-28]. Recently, Wang and co-workers [28] have observed a strong influence of the particle size on both the charcoal and fixed-carbon yields at pressures ranging from 0.1 to 2.7 MPa. Increasing the particle size is a mean to prolong the contact between the vapor-phase species with the solid in the interior of the particle. Thus, an enhancement of the secondary reactions, which leads to an increase in the fixed-carbon yield, can be expected when the particle size is larger.

It should be kept in mind that, in addition to the above-discussed operating parameters; the intrinsic properties of the biomass feedstock (such as moisture content, ash content and composition, and extractives and lignin contents) may also strongly affect the course of the pyrolysis process [6,14,29]. For this reason, experimental findings on biomass pyrolysis cannot be generalized to a wide range of materials.

The primary aim of the present study is to evaluate the effect of the pressure, peak temperature, and particle size on the potential stability of the biochar produced by slow pyrolysis

of vine shoots. The wine industry generates large amounts of agricultural wastes (particularly vine shoots and leaves). Assuming that one hectare of vines yields 1.4–2.0 tons of shoots and that the vineyard cultivated area in the world is over 8 million ha, an annual production of 11–16 million tons of vine shoots is estimated [30]. The most important aspect of the study reported here is that pyrolysis experiments were conducted at constant inert gas residence time by adjusting the inert gas mass flow rate as a function of both the pressure and temperature in the pyrolysis reactor. This fact will allow us to estimate the intrinsic effect of pressure. A 2-level factorial design of experiments was adopted to objectively analyze the effects of the above-mentioned factors and the interactions among them. Using this approach, statistically significant effects can be identified and, thus, valuable guidance can be provided to the research community. Experimental runs were performed in a pressurized fixed-bed slow-pyrolysis unit.

2. Experimental Section

2.1. Materials

The vine shoots used in the present study were supplied by a wine company located in the wine region of Somontano (Spain). The original material was crushed and then sieved (through an ASTM E11-95 sieve stack) to obtain three different mean particle sizes (0.98, 1.97, and 3.01 cm). Table 1 shows the results of the proximate, elemental, and XRF analyses of the samples. The proximate analyses were performed in quadruplicate according to ASTM standards (D3173 for moisture, D3174 for ash, and D3175 for volatile matter), whereas the elemental analyses were carried out using a Leco TruSpec Micro CHNS analyzer (Leco Corporation, St. Joseph, MI). An ADVANT'XP+ XRF spectrometer (Thermo ARL, Switzerland) was used to measure the ash composition on the basis of the weight fractions of the equivalent oxides [31] according to ASTM standard D4326-04.

2.2. Experimental system

The experimental system used in the present study, the diagram of which is given in Fig. 1, is able to work under an absolute pressure of up to 1.5 MPa and at inlet temperatures (in the pyrolysis reactor) of up to 800 °C. The pyrolysis reactor consists of a vertical tube (40.9 mm ID; 500 mm long) made of high temperature austenitic stainless steel (Outokumpu 253™; EN 1.4835) and electrically heated using a 0.9 kW electric resistance with PID temperature control. In order to remove the maximum amount of tar from the exit gas stream, the cracking reactor (a vertical tube of 20.9 mm ID and 250 mm long, made of ASTM 316L stainless steel, and electrically heated by a 0.5 kW resistance) contains a fixed-bed of alumina porous particles at an inlet temperature of about 700 °C. The activated aluminum oxide used in this study was Compalox® AN/V-812 (particle size of 1.0–2.5 mm and BET specific surface area of 230–300 $m^2\ g^{-1}$) from Albemarle (Germany). An electrically heated filter, consisting of a tubular ASTM 316L stainless steel body that holds a glass fiber thimble, was placed at the exit of the cracking reactor to remove solid particles. The temperature inside the filter, as well as on the trace-heated connecting tubes, was maintained at 400–450 ºC to prevent tar condensation. The liquid product (water and tar) was condensed in a glass trap immersed in an ice-water bath. The gaseous product was analyzed using a micro gas chromatograph (μ-GC Varian CP-4900) equipped with two independent channels and thermal conductivity detectors. Gas sample injections were started when a pyrolysis reactor temperature of 250 °C was reached.

The pressure of the system was controlled by a back pressure regulator. The inert (N_2) mass flow rate through the pyrolysis reactor was adjusted as a function of the pressure and temperature (measured by means of a K-type thermocouple placed at the cylinder axis and 5 cm from the bottom of the reactor) to maintain the superficial gas velocity constant at 0.015 m s^{-1}, which results (assuming a void fraction of 0.5 for both reactors) in a gas hourly space velocity (GHSV) of 216 h^{-1} and 1230–1595 h^{-1} for the pyrolysis and cracking reactors, respectively.

For each experimental run, approximately 30 g of vine shoots were charged to the fixed-bed pyrolysis reactor at room conditions. After checking for absence of leaks, the system was pressurized with nitrogen at the desired pressure. The N_2 mass flow rate was continuously adjusted by means of a mass flow controller. The inert gas was heated to 350 °C in a preheater unit (a coiled tube with a resistive wire of 0.25 kW) and then fed to the pyrolysis reactor through the distribution plate. The pyrolysis reactor was heated to the desired peak temperature at a heating rate of about 5 K min^{-1}. Each experimental run was completed 1 hour after the pyrolysis peak temperature was reached. During the natural cooling of the device, the N_2 flow was maintained to prevent charcoal oxidation. Once the pyrolysis reactor reached room temperature, the gas flow was turned-off and the system depressurized. The liquid fraction and biochar were then weighted to determine the respective yields. The water content in the liquid product was measured by Karl-Fischer titration, whereas the gas yield was estimated from the overall mass balance.

2.3. Biochar characterization

The obtained biochars were characterized by proximate and elemental analyses, according to the same above-mentioned procedures. The pH of the biochars was measured in deionized water at 1:5 (wt/wt) ratio after stirring for 1 hour [32]. In order to estimate the proportion of aromatic carbon, solid-state ^{13}C CP-MAS nuclear magnetic resonance (NMR) spectra were obtained for all the biochar samples using a Bruker Avance 400 (Bruker Corp., Germany) spectrometer at a frequency of 100 MHz. Adopting the approach previously used by McBeath and co-workers [16], the proportion of aromatic carbon was estimated as the ratio of the area under the aromatic peaks to the total area of the NMR spectrum. A preliminary deconvolution procedure, consisting in fitting the experimental signal as the sum of multiple Gaussian peaks, was performed using the “Peak Analyzer” tool implemented in OriginPro version 8.5 (OriginLab, Northampton, MA).

The fitted peaks were then attributed to aromatic carbon in the case that the center of the peak was in the chemical shift range of 110–165 ppm.

The proportion of aromatic carbon deduced from the NMR spectra is a good indicator of the potential stability of biochar in the soil [3]. Recently, Singh and co-workers [33] observed that both the labile fraction of carbon in biochar and the estimated mean residence time of biochar in the soil were positively correlated with the proportion of aromatic C.

2.4. Design of experiments

Factorial designs are most efficient designs to study the joint effect of two or more factors on a response [34]. The most widely used of these designs are the 2-level factorial designs, which provide the smallest number of runs to estimate both the main and interaction effects the selected factors. An unreplicated 2-level factorial design [34] was adopted in the present study to statistically evaluate the effects of the three main factors (absolute pressure, peak temperature, and particle size). The RcmdrPlugin.DoE package [35] within the R environment (version 3.0.1) was used to generate the design of experiments and perform the appropriate statistical analyses. To estimate the intrinsic experimental error and, simultaneously, the overall curvature effect; three replicates at the center point were carried out. Table 2 shows the matrix of the randomly generated design.

The following response variables, all of them related to biochar characteristics, were statistically evaluated: the mass yield in a dry basis (y_{char}), the fixed-carbon yield (y_{FC}) in a dry and ash-free basis and calculated according to Eq. (1), the molar H:C ratio, the molar O:C ratio, the percentage of aromatic C, and the pH.

$$y_{FC} = \left(\frac{m_{char}}{m_{bio}}\right)\left(\frac{\%FC}{100-\%ash}\right) \quad (1)$$

In Eq. (1), *%FC* and *%ash* are the percentage of fixed-carbon present in the biochar and the percentage of ash in the feedstock, respectively; whereas the ratio between m_{char} (mass of produced biochar) and m_{bio} (dry mass of feedstock) is equal to the biochar yield (y_{char}). The y_{FC}

value is a good indicator of the efficiency of the pyrolytic conversion of the ash-free organic matter (initially present in the biomass feedstock) to a relatively pure, ash-free carbon [12]. In addition to this, the fixed-carbon yield could also be an additional measure of the potential stability of the produced biochar, as recently confirmed by Zimmerman [36], who found a significant positive correlation between the labile fraction of carbon and the volatile matter content of biochar.

3. Results and discussion

Table 3 summarizes the main experimental results. For each response, a regression model including the linear and the linear interaction terms was estimated. Thus, from the experimental data obtained, functional relationships between the response (y) and the coded independent variables (x_1 for pressure, x_2 for peak temperature, and x_3 for particle size) can be quantified by means of the estimated parameters of the regression model:

$$y = \beta_0 + \sum_{j=1}^{k} \beta_j x_j + \sum_{i<j} \sum \beta_{ij} x_i x_j + \varepsilon \quad (2)$$

where β_0, β_j, and β_{ij} are the intercept, linear, and interaction coefficients; respectively. Statistical significance of model terms was evaluated using parametric tests (t-test). In the event that the curvature term is found to be significant (i.e., p-value < 0.05), the linear regression model may be not accurate enough and a second-order regression model that includes the quadratic terms is probably required. The results of the statistical analyses are given in Table 4.

3.1. Biochar and fixed-carbon yields

From the results reported in Table 4, it is deduced that the biochar yield (y_{char}) is statistically affected (at a 95% of confidence level) by the peak temperature, the particle size and the interaction between them. Hence, the effect of the pressure on this response is not significant.

Since the curvature term was not significant, the linear regression model can be accurate enough to predict the product mass yield (see Fig. 2 for the corresponding 2-factor contour plots).

In regard to the effects on the fixed-carbon yield, significant changes are only observed for the particle size and its interaction with peak temperature. In this case, the overall curvature was significant and, consequently, the linear regression model could be not predictive. For this reason, contour plots cannot be used. However, the 2-interaction effect plots are shown in Fig. 3. From these plots, the same conclusions deduced from Table 4 can be drawn visually: the significant increase in fixed-carbon yield as the particle size increases and the presence of a marked curvature.

In addition to the expected effect of the peak temperature on the biochar yield (i.e., a significant decrease in y_{char} with the rise of the peak temperature), the results obtained in the present study reveal that the particle size is the key factor in determining the fixed-carbon yield. This fact suggests that the residence time of the primary tar vapors inside the particle is the main responsible for the enhancement of the secondary reactions, which lead to an additional formation of carbon through repolymerization. Increasing the peak temperature at the highest level of the particle size factor causes a supplementary increase in the y_{FC} value. For its part, the absolute pressure (keeping constant the gas residence time in the bed) does not significantly affect either the biochar or fixed-carbon yields. At this point, it is important to highlight that these results are restricted to the specific biomass feedstock and the range of operating conditions used in this study.

On the other hand, it should be pointed out that the selection of the operating conditions required to maximize the fixed-carbon yield (the highest peak temperature and the highest particle size) does not result in the minimization of the biochar yield. This fact demonstrates the unreliability of the biochar yield as an indicator of the potential stability of biochar.

3.2. Aromaticity, H:C and O:C ratios, and pH

As can be seen from the data reported in Table 4 and the interaction plots shown in Fig. 4, the percentage of aromatic carbon significantly increases as the particle size and/or the peak temperature rises. The effect of the peak temperature is in good agreement with previous works [14,16-18], whereas the effect of the particle size indicates that the operating conditions that maximize the fixed-carbon yield also maximize the content of aromatic carbon in the produced biochar. In fact, these responses variables are linearly correlated as shown in Table 5. In addition, results indicate no statistically significant effects of increasing pressure on the aromaticity of biochar. This finding may seem to be in disagreement with the earlier study of Melligan and co-workers [24], who observed an increase of the aromatic carbon content with pressure. Nevertheless, it should be noted that Melligan and co-workers performed all of the experiments at a constant N_2 mass flow rate, that is, at a variable gas residence time in the pyrolysis reactor.

As for the fixed-carbon yield, the regression coefficient of the overall curvature term for the percentage of aromatic carbon was significant (p-value = 0.012). This curvature can also be visualized in Fig. 4. The presence of curvature for the two correlated responses (fixed-carbon yield and percentage of aromatic carbon) suggests that a central composite design (obtained by expanding the current factorial design) could be required to estimate the quadratic regression coefficients.

Regarding the behavior of the molar H:C and O:C ratios, no significant effects of any of the factors were found. Despite the fact that the general trend of both molar ratios with increasing peak temperature are in good agreement with previous results reported in the literature [13,17,19,37] (see β_2 values listed in Table 4), no statistically robust conclusions can be drawn. However, from the Pearson's correlation matrix given in Table 5, it can be seen that both ratios are negatively correlated with the percentage of aromatic carbon, as expected. This outcome might suggest that additional factors (such as the holding time at peak temperature and the N_2

superficial velocity through the bed) can partly explain these responses. In addition to this, it is important to highlight that the molar H:C and O:C ratios obtained for the best treatment (x_2 = 1, x_3 = 1; runs #5 and #9) are relatively high in comparison to those reported in previous studies. For example, Ghani and co-workers [19] reported molar H:C and O:C ratios of 0.33 and 0.06, respectively; for biochars obtained at 550 °C from rubber-wood sawdust. Similar values were measured by Keiluweit and co-workers [37] (for pine shavings-derived biochar obtained at a peak temperature of 600 °C), Wu and co-workers [17] (for rice straw-derived biochar obtained at 600 °C), and Kim and co-workers [38] (for pitch pine chips-derived biochar at 500 °C). More in line with the results described here, Enders and co-workers [13] measured molar H:C and O:C ratios of 0.45 and 0.10, respectively; for biochars produced by slow pyrolysis of corn stover at 600 °C. This variability of results may be explained by the intrinsic properties of the biomass feedstock (i.e., chemical composition), and partly also by differences in process conditions during the thermal decomposition. In this respect, the holding time at the peak temperature can play a critical role in the carbonization efficiency, especially in the cases where the heat transfer limitations at all scales (inter- and intra-particle) are not negligible. Thus, the solid residence time at the peak temperature used in the present study (1 h) is probably not long enough to complete the carbonization process.

Concerning the effects on the pH of biochar, the statistics given in Table 4 indicates that this response is only significantly affected by the particle size (at a confidence level of 95%). Fig. 5 displays the contour plots described by the linear regression model (the coefficient corresponding to the overall curvature is not significant). Unexpectedly, the effect of peak temperature on the pH was not significant (p-value = 0.069), in disagreement with the general trend (an increase in pH as the peak temperature raised) deduced from the results of numerous earlier studies [13,17,32,39]. Enders and co-workers [13] attributed the increase in pH to a decrease in acid functional groups for low-ash biochars (like those used in the present study, with ash contents of 5.44% ± 2.54%). In this sense, no linear correlation has been found between

the pH and the ash content for the biochars produced here (ρ = 0.354; p-value = 0.286). Hence, the loss of acidic functional groups in surface seems to be the main cause of the increase in pH.. This result seems to be logical because the promotion of secondary tar reactions (at the intra-particle level) leads to more aromatic functional groups (see statistical analysis for the percentage of aromatic carbon in Table 4). It should be stated that a decrease in acid functional groups can imply a decrease in the cation exchange capacity (CEC), as mentioned in previous works [17,39]. In other words, the application of the most stable biochar (which also has the maximum pH value) to soil might not be the best alternative to optimize the retention of nutrients. Nevertheless, further studies are required to investigate the evolution of both the pH and CEC when biochar is added to a given type of soil. Among other variables, the initial acidity of the soil will probably be a key factor in determining the most appropriate biochar from an agronomic point of view.

3.3. Gas yield and composition

Table 4 also shows the regression coefficients for the following additional responses: the mass yields of pyrolysis gas, water, and tar in a dry basis (y_{gas}, y_{water}, and, y_{tar}; respectively), and the average contents (in vol %) of the major components in the producer gas (in a dry and inert-gas free basis).

As can be deduced from the data reported in Table 4, the gas yield significantly increases with the peak temperature due to the expected promotion of the devolatilization process. When the peak temperature is fixed at its highest value (600 °C), pressure slightly favors the gas production (β_{12} = 0.021; p-value = 0.038). Particularly interesting is the effect of the particle size, because the interaction with the peak temperature was more significant than the main effect of this factor alone. In other words, using smaller particles and operating under high pressure and at a high peak temperature is the best way to maximize the pyrolysis gas production. This combination also leads to the expected minimization of the biochar yield (ρ = –0.974; p-value = 0.000).

With regard to the water and tar yields (which are linearly correlated: ρ = 0.792; p-value = 0.004), all of the regression coefficients were statistically significant (at a 95% of confidence level) including those corresponding to the 2-factor interactions. Pressure enhances the tar cracking in the bed of activated alumina particles, probably as a result of an increase in the adsorption capacity of condensable molecules. The particle size also decreases the formation of tar as a consequence of the higher conversion of vapor tars into gas and charcoal via intra-particle secondary reactions. The positive effect of pressure on decreasing the liquid fraction yield was also reported by Seshadri and Shamsi [40] and, more recently, by Ragucci and co-workers [41]. As a general remark, it can be noted that the average tar yield given in Table 4 (β_0 = 1.33 g kg^{-1} dry biomass) is about two orders of magnitude lower than the usual values reported in the literature for slow pyrolysis systems without using a separate tar cracking step [42–44].

Despite the fact that the behavior of the multiple reactions involved in the cracking reactor is very difficult to predict in practice, some interesting considerations can be drawn from the results shown in Table 4. First, the increase of the methane content in the exit gas with pressure is an expected result, because of the beneficial effect of this factor on the methanation reaction (Eq. 3).

$$CO + 3H_2 \leftrightarrow CH_4 + H_2O \quad (3)$$

$$CO + H_2O \leftrightarrow CO_2 + H_2 \quad (4)$$

$$C + 2H_2 \leftrightarrow CH_4 \quad (5)$$

$$CO_2 + C \leftrightarrow 2CO \quad (6)$$

Second, the water generated during the methanation inside the cracking reactor could promote the water-gas-shift (WGS) reaction (Eq. 4). This argument may explain the significant decrease in the water yield and CO content with increasing pressure. Third, the production of hydrogen significantly decreases with increasing pressure when the peak temperature is set at its highest level (β_{12} = –8.79; p-value = 0.007). This fact can be due to the enhancement under pressure of

the methanation of coke (Eq. 5), which was previously deposited on the surface of the alumina particles. Finally, it should be noted that the particle size also affects the hydrogen and carbon monoxide contents in the produced gas. The H_2 production is significantly enhanced when the peak temperature and the particle size are set at their highest levels (β_{23} = 4.02; p-value = 0.034), probably as a consequence of an additional release of H_2 via secondary pyrolysis of the tar vapors. On the other hand, the CO yield is also favored when larger particles of vine shoots are used. One possible explanation for this result is that the progress of the inverse Boudouard reaction (Eq. 6) is enhanced with the increase of the gas residence time inside the particle.

4. Conclusions

From the experimental results obtained in the present study, the following conclusions seem justified:

(1) Among the three factors statistically evaluated, the most influential was the particle size under the experimental conditions used in this study. Operating with larger particles leads to a simultaneous increase in the fixed-carbon yield, the percentage of aromatic carbon, and the pH. Thus, the potential stability of the vine shoots-derived biochar is mainly determined by the particle size. This finding is interesting from both operational and economic points of view, because the size reduction step can be simplified or avoided.

(2) For the biomass feedstock and the range of operating factors (a relatively small range of pressure values and a constant inert gas residence time inside the pyrolysis reactor) used in our study, the absolute pressure did not play any significant role in the potential stability of the produced biochar. Hence, alternative ways to increase the contact time between the tar vapors and the carbonaceous solid, such as the use of large particles, can be effective as well.

(3) As expected, an increase of the peak temperature caused a significantly increase in the aromaticity of the biochar. However, the positive effect of the peak temperature on the fixed-carbon yield is less pronounced and only significant when larger particles of vine shoots were

used. For both responses, the regression coefficients corresponding to the overall curvature were significant. Thus, the linear regression model is probably not accurate enough to explain the data and a second-order design (e.g., a central composite design) is needed to better determine the effects of the above-mentioned factors.

(4) Using a bed of activated alumina particles represents a low-cost way to partly remove tar and simultaneously improve the product gas yield and composition. The tar content in the exit gas was minimized when all of the factors (including the pressure) were fixed at their highest levels. Increasing both the peak temperature and particle size also led to a higher production of gas.

(5) The highest hydrogen content (around 40 vol %) was obtained when the largest particles of vine shoots were pyrolyzed under atmospheric pressure and at the highest peak temperature. This promising finding requires further research initiatives to explore the possibility of producing hydrogen from the pyrolysis gas thought CO and CH_4 conversion and subsequent CO_2 capture.

Acknowledgements

J.J.M. gratefully acknowledges financial support from the University of Zaragoza (Project UZ2012-TEC-04). The authors gratefully thank Dr. Ignacio Delso for his excellent work in performing the NMR measurements.

Nomenclature

$GHSV$ = gas hourly space velocity (h^{-1})

m_{bio} = dry mass of biomass sample (kg)

m_{char} = mass of produced biochar (kg)

R^2_{adj} = adjusted coefficient of determination

x_1 = coded variable for pressure

x_2 = coded variable for peak temperature

x_3 = coded variable for particle size

y_{char} = biochar yield (kg kg^{-1} of biomass in a dry basis)

y_{FC} = fixed-carbon yield (kg kg^{-1} of biomass in a dry and ash-free basis)

y_{gas} = yield of producer gas (kg kg^{-1} of biomass in a dry and N_2-free basis)

y_{water} = yield of water (g kg^{-1} of biomass in a dry basis)

y_{tar} = yield of tar (g kg^{-1} of biomass in a dry basis)

Greek Symbols

β_0 = regression coefficient for the intercept term

β_1 = regression coefficient for the linear effect of pressure

β_2 = regression coefficient for the linear effect of peak temperature

β_3 = regression coefficient for the linear effect of particle size

β_{12} = regression coefficient for the interaction term between pressure and peak temperature

β_{13} = regression coefficient for the interaction term between pressure and particle size

β_{23} = regression coefficient for the interaction term between peak temperature and particle size

β_{11} = regression coefficient for the quadratic effect of peak temperature

ρ = Pearson's correlation coefficient

Acronyms

BET = Brunauer Emmett Teller

CEC = cation exchange capacity

CP-MAS = cross polarization and magic angle spinning

FC = fixed carbon

GC = gas chromatography

NMR = nuclear magnetic resonance

PID = proportional integral derivative

RSM = response surface methodology

TGA = thermogravimetric analysis

XRF = X-ray fluorescence

WGS = water gas shift

References

[1] Gaunt JL, Lehmann J. Energy balance and emissions associated with biochar sequestration and pyrolysis bioenergy production. Environ Sci Technol 2008;42:4152–8.

[2] McHenry MP. Agricultural bio-char production, renewable energy generation and farm carbon sequestration in Western Australia: Certainty, uncertainty and risk. Agric Ecosyst Environ 2009;129:1–7.

[3] Manyà JJ. Pyrolysis for biochar purposes: a review to establish current knowledge gaps and research needs. Environ Sci Technol 2012;46:7939–54.

[4] Zhang L, Chunbao X, Champagne P. Overview of recent advances in thermo-chemical conversion of biomass. Energy Conv Manage 2010;51:969–82.

[5] Brewer CE, Schmidt-Rohr K, Satrio JA, Brown RC. Characterization of biochar from fast pyrolysis and gasification systems. Environ Prog Sustainable Energy 2009;28:386–96.

[6] Antal MJ, Gronli M. The art, science, and technology of charcoal production. Ind Eng Chem Res 2003;42:1619–40.

[7] Di Blasi C, Signorelli G, Di Russo C, Rea G. Product distribution from pyrolysis of wood and agricultural residues. Ind Eng Chem Res 1999;38:2216–24.

[8] Demirbas A. Effects of temperature and particle size on bio-char yield from pyrolysis of agricultural residues. J Anal Appl Pyrolysis 2004;72:243–8.

[9] Abdullah H, Wu H. Biochar as a fuel: 1. Properties and grindability of biochars produced from the pyrolysis of mallee wood under slow-heating conditions. Energy Fuels 2009;23:4174–81.

[10] Duman G, Okutucu C, Ucar S, Stahl R, Yanik J. The slow and fast pyrolysis of cherry seed. Bioresour Technol 2011;102:1869-78.

[11] Méndez A, Terradillos M, Gascó G. Physicochemical and agronomic properties of biochar from sewage sludge pyrolysed at different temperatures. J Anal Appl Pyrolysis 2013;102:124–30.

[12] Antal MJ, Allen SG, Dai X, Shimizu B, Tam MS, Gronli M. Attainment of the theoretical yield of carbon from biomass. Ind Eng Chem Res 2000;39:4024–31.

[13] Enders A, Hanley K, Whitman T, Joseph S, Lehmann J. Characterization of biochars to evaluate recalcitrance and agronomic performance. Bioresour Technol 2012;114:644–53.

[14] Zhao L, Cao X, Mašek O, Zimmerman A. Heterogeneity of biochar properties as a function of feedstock sources and production temperatures. J Hazard Mater 2013;256–257:1–9.

[15] Manyà JJ, Roca FX, Perales JF. TGA study examining the effect of pressure and peak temperature on biochar yield during pyrolysis of two-phase olive mill waste. J Anal Appl Pyrolysis 2013;103:86–95.

[16] McBeath AV, Smernik RJ, Schneider MPW, Schmidt MWI, Plant EL. Determination of the aromaticity and the degree of aromatic condensation of a thermosequence of wood charcoal using NMR. Org Geochem 2011;42:1194–202.

[17] Wu W, Yang M, Feng Q, et al. Chemical characterization of rice straw-derived biochar for soil amendment. Biomass Bioenergy 2012;47:268–76.

[18] Sun H, Hockaday WC, Masiello CA, Zygourakis K. Multiple controls on the chemical and physical structure of biochars. Ind Eng Chem Res 2012;51:3587–97.

[19] Ghani WAWAK, Mohd A, da Silva G, et al. Biochar production from waste rubber-wood-sawdust and its potential use in C sequestration: Chemical and physical characterization. Ind Crops Prod 2013;44:18–24.

[20] Pindoria RV, Megaritis A, Messenböck RC, Dugwell DR, Kandiyoti R. Comparison of the pyrolysis and gasification of biomass: effect of reacting gas atmosphere and pressure on Eucalyptus wood. Fuel 1998;77:1247–51.

[21] Mok WS, Antal MJ. Effects of pressure on biomass pyrolysis. I. Cellulose pyrolysis products. Thermochim Acta 1983;68:155–64.

[22] Antal MJ, Croiset E, Dai X, et al. High-yield biomass charcoal. Energy Fuels 1996;10:652–8.

[23] Elyounssi K, Blin J, Halim M. High-yield charcoal production by two-step pyrolysis. J Anal Appl Pyrolysis 2010;87:138–43.

[24] Melligan F, Auccaise R, Novotny EH, Leahy JJ, Hayes MHB, Kwapinski W. Pressurised pyrolysis of Miscanthus using a fixed bed reactor. Bioresour Technol 2011;102:3466–70.

[25] Shen J, Wang X, Garcia-Perez M, Mourant D, Rhodes MJ, Li C. Effects of particle size on the fast pyrolysis of oil mallee woody biomass. Fuel 2009;88:1810–7.

[26] Luangkiattikhun P, Tangsathitkulchai C, Tangsathitkulchai M. Non-isothermal thermogravimetric analysis of oil-palm solid wastes. Bioresour Technol 2008;99:986–97.

[27] Haykiri-Acma H. The role of particle size in the non-isothermal pyrolysis of hazelnut shell. J Anal Appl Pyrolysis 2006;75:211–6.

[28] Wang L, Skreiberg A, Gronli M, Specht GP, Antal MJ. Is elevated pressure required to achieve a high fixed-carbon yield of charcoal from biomass? Part 2: the importance of particle size. Energy Fuels 2013;27:2146–56.

[29] Burhenne L, Messmer J, Aicher T, Laborie M. The effect of the biomass components lignin, cellulose and hemicellulose on TGA and fixed bed pyrolysis. J Anal Appl Pyrolysis 2013;101:177–84.

[30] Peralbo-Molina A, Luque de Castro MD. Potential of residues from the Mediterranean agriculture and agrifood industry. Trends Food Sci Technol 2013;32:16–24.

[31] Liao C, Wu C, Yan Y. The characteristics of inorganic elements in ashes from a 1 MW CFB biomass gasification power generation plant. Fuel Process Technol 2007;88:149–56.

[32] Yuan J, Xu R, Zhang H. The forms of alkalis in the biochar produced from crop residues at different temperatures. Bioresour Technol 2011;102:3488–97.

[33] Singh BP, Cowie AL, Smernik RJ. Biochar carbon stability in a clayey soil as a function of feedstock and pyrolysis temperature. Environ Sci Technol 2012;46:11770–8.

[34] Montgomery DC. Design and analysis of experiments. Hoboken, NJ: John Wiley & Sons, 2005.

[35] Grömping U. Tutorial for designing experiments using the R package RcmdrPlugin.DoE, Report 4/2011, Reports in Mathematics, Physics and Chemistry, Berlin: Beuth University of Applied Sciences; 2011.

[36] Zimmerman AR. Abiotic and microbial oxidation of laboratory-produced black carbon (biochar). Environ Sci Technol 2010;44:1295–301.

[37] Keiluweit M, Nico PS, Johnson MG, Kleber M. Dynamic molecular structure of plant biomass-derived black carbon (biochar). Environ Sci Technol 2010;44:1247–53.

[38] Kim KH, Kim J, Cho T, Choi JW. Influence of pyrolysis temperature on physicochemical properties of biochar obtained from the fast pyrolysis of pitch pine (Pinus rigida). Bioresour Technol 2012;118:158–62.

[39] Mukherjee A, Zimmerman AR, Harris W. Surface chemistry variations among a series of laboratory-produced biochars. Geoderma 2011;163:247–55.

[40] Seshadri KS, Shamsi A. Effects of temperature, pressure, and carrier gas on the cracking of coal tar over a char-dolomite mixture and calcined dolomite in a fixed-bed reactor. Ind Eng Chem Res 1998;37:3830–7.

[41] Ragucci R, Giudicianni P, Cavaliere A. Cellulose slow pyrolysis products in a pressurized steam flow reactor. Fuel 2013;107:122–30.

[42] Phuphuakrat T, Namioka T, Yoshikawa K Tar removal from biomass pyrolysis gas in two-step function of decomposition and adsorption. Appl Energy 2010;87:2203-11.

[43] Sun Q, Yu S, Wang F, Wang J Decomposition and gasification of pyrolysis volatiles from pine wood through a bed of hot char. Fuel 2011;90:1041-8.

[44] Adrados A, Lopez-Urionabarrenechea A, Solar J, Requies J, De Marco I, Cambra JF Upgrading of pyrolysis vapours from biomass carbonization. J Anal Appl Pyrolysis 2013;103:293-9.

Table 1

Proximate, elemental, and XRF analyses of the vine shoots

Proximate (wt %)	
Ash	2.46 ± 0.37
Moisture	10.47 ± 0.13
Volatile Matter	72.93 ± 1.64
Fixed Carbon	14.14 ± 1.38
Elemental (wt %, dry and ash-free basis)	
C	42.3 ± 0.37
H	5.70 ± 0.16
N	1.28 ± 0.17
S	< 0.1
Inorganic matter (wt % of ash)	
CaO	58.3
K_2O	18.4
SiO_2	5.73
Fe_2O_3	3.51
Al_2O_3	2.57
P_2O_5	1.24
MgO	6.66
TiO_2	0.336
PbO	0.260
SnO_2	0.256
CuO	0.089
MnO	0.532
ZnO	0.332
SO_3	0.601
Cl	0.475

Table 2

Matrix of the 2^3 factorial design adopted in the present study

Level	Factors		
	$\mathbf{x_1}$	$\mathbf{x_2}$	$\mathbf{x_3}$
	Pressure (MPa)	Peak Temperature (°C)	Sample size (cm)
Low (–1)	0.1	400	0.2–1.0
Middle (0)	0.6	500	0.4–2.0
High (+1)	1.1	600	0.6–3.0
Run	Factors		
	$\mathbf{x_1}$	$\mathbf{x_2}$	$\mathbf{x_3}$
1	1	–1	1
2	0	0	0
3	0	0	0
4	–1	1	–1
5	1	1	1
6	–1	–1	1
7	1	1	–1
8	1	–1	–1
9	–1	1	1
10	–1	–1	–1
11	0	0	0

Table 3

Experimental results obtained from the 2-level fractional design

Run	y_{char}	y_{FC}	*Aromatic C (%)*	*H:C molar ratio*	*O:C molar ratio*	*pH*
1	0.5671	0.3301	47.80	0.739	0.275	9.20
2	0.5481	0.2384	27.80	0.967	0.440	8.66
3	0.5442	0.2440	27.70	0.793	0.345	8.76
4	0.5099	0.2293	41.98	0.833	0.259	8.55
5	0.5504	0.3920	66.70	0.518	0.174	8.84
6	0.5396	0.3243	57.90	0.694	0.207	8.94
7	0.4360	0.2201	49.18	0.746	0.198	8.65
8	0.7797	0.2561	30.23	1.004	0.360	8.62
9	0.5256	0.3618	60.50	0.607	0.108	8.75
10	0.6784	0.2473	31.78	0.772	0.224	8.59
11	0.5885	0.2619	33.15	0.788	0.304	8.75

Table 4

Summary statistics for the regression models (values in brackets correspond to the *p*-values obtained from the hypothesis tests)

Response	β_0	β_1	β_2	β_3	β_{12}	β_{13}	β_{23}	*Curvature*[a]	R^2_{adj}[b]
y_{char}	0.5698	0.0100	–0.0679	–0.0277	–0.0222	0.0031	0.0602	–0.0131	0.9267
	(0.000)	(0.307)	(0.004)	(0.042)	(0.071)	(0.727)	(0.005)	(0.514)	
y_{FC}	0.2951	0.0044	0.0057	0.0569	0.0008	0.0046	0.0192	–0.0470	0.9456
	(0.000)	(0.413)	(0.321)	(0.006)	(0.871)	(0.404)	(0.048)	(0.030)	
Molar H:C ratio	0.739	0.013	–0.063	–0.099	–0.057	–0.024	–0.014	0.110	0.4693
	(0.002)	(0.760)	(0.222)	(0.110)	(0.257)	(0.579)	(0.737)	(0.251)	
Molar O:C ratio	0.235	0.017	–0.032	–0.026	–0.034	–0.002	–0.000	0.128	0.3288
	(0.011)	(0.559)	(0.325)	(0.408)	(0.303)	(0.953)	(0.996)	(0.113)	
Aromatic C (%)	48.26	0.22	6.33	9.97	3.13	–1.19	–0.96	–18.71	0.9515
	(0.001)	(0.861)	(0.029)	(0.012)	(0.105)	(0.392)	(0.477)	(0.012)	
pH	8.77	0.06	–0.07	0.17	–0.01	0.03	–0.07	–0.04	0.9126
	(0.000)	(0.091)	(0.069)	(0.014)	(0.587)	(0.293)	(0.074)	(0.358)	
y_{gas}[c]	0.392	0.006	0.067	0.041	0.021	–0.007	–0.056	0.021	0.9835
	(0.000)	(0.285)	(0.004)	(0.010)	(0.038)	(0.247)	(0.005)	(0.118)	
y_{water}[d]	17.0	–6.47	3.17	–5.08	–0.323	–1.14	–3.30	–9.20	0.9997
	(0.000)	(0.000)	(0.000)	(0.000)	(0.026)	(0.002)	(0.000)	(0.000)	
y_{tar}[d]	1.33	–0.633	0.272	–0.760	–0.348	0.354	–0.525	–0.407	0.9963
	(0.000)	(0.002)	(0.009)	(0.001)	(0.005)	(0.005)	(0.002)	(0.014)	

[a] Regression coefficient for the overall curvature

[b] Calculated for the regression model that includes the curvature term

[c] In kg kg^{-1} dry biomass

[d] In g kg^{-1} dry biomass

Table 4

(continued)

Response	β_0	β_1	β_2	β_3	β_{12}	β_{13}	β_{23}	*Curvature*[a]	R^2_{adj}[b]
H_2 (% vol)	24.5	1.50	3.08	–2.29	–8.79	–2.82	4.02	11.6	0.9639
	(0.001)	(0.189)	(0.057)	(0.096)	(0.007)	(0.066)	(0.034)	(0.016)	
CO (% vol)	24.3	–2.40	0.035	2.36	4.45	1.64	–1.68	–8.35	0.9790
	(0.000)	(0.023)	(0.933)	(0.024)	(0.007)	(0.047)	(0.045)	(0.007)	
CO_2 (% vol)	34.7	–1.88	–5.41	–2.63	2.04	–1.97	1.08	–5.25	0.9237
	(0.000)	(0.117)	(0.017)	(0.065)	(0.102)	(0.108)	(0.265)	(0.060)	
CH_4 (% vol)	15.08	2.89	2.55	2.71	1.94	3.22	–3.69	0.324	0.9945
	(0.000)	(0.003)	(0.004)	(0.004)	(0.008)	(0.003)	(0.002)	(0.427)	

Table 5

Pearson's correlation matrix for selected response variables (values in brackets correspond to the *p*-values obtained from the hypothesis tests)

	y_{char}	y_{FC}	*Aromatic C (%)*	*H:C molar ratio*	*O:C molar ratio*
y_{FC}	–0.062				
	(0.857)				
Aromatic C (%)	–0.454	0.802			
	(0.160)	(0.003)			
H:C molar ratio	0.463	–0.766	–0.851		
	(0.151)	(0.006)	(0.001)		
O:C molar ratio	0.349	–0.534	–0.821	0.850	
	(0.292)	(0.091)	(0.002)	(0.001)	
pH	–0.156	0.626	0.431	–0.420	–0.175
	(0.647)	(0.040)	(0.185)	(0.199)	(0.606)

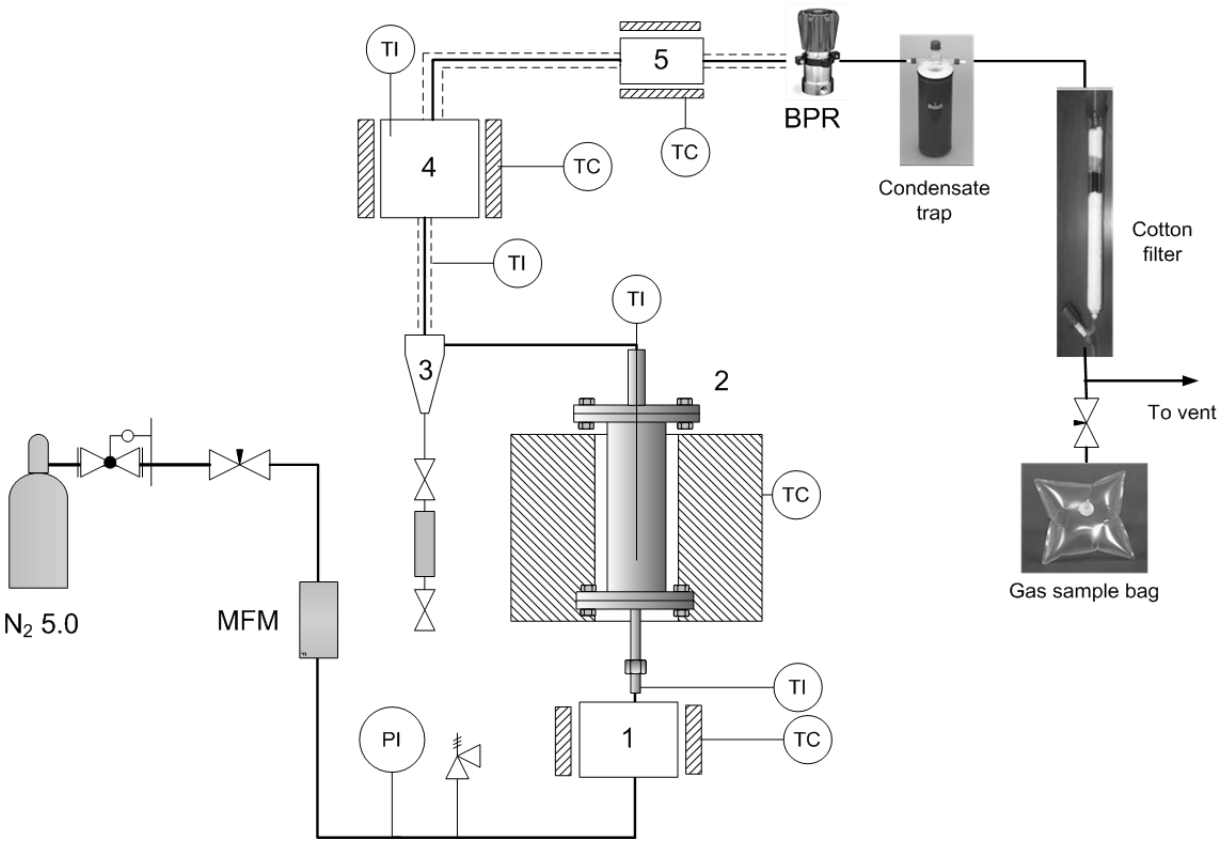

Fig. 1. Schematic diagram of the experimental system: (1) preheater, (2) fixed-bed pyrolysis reactor, (3) cyclone, (4) cracking reactor, and (5) hot filter.

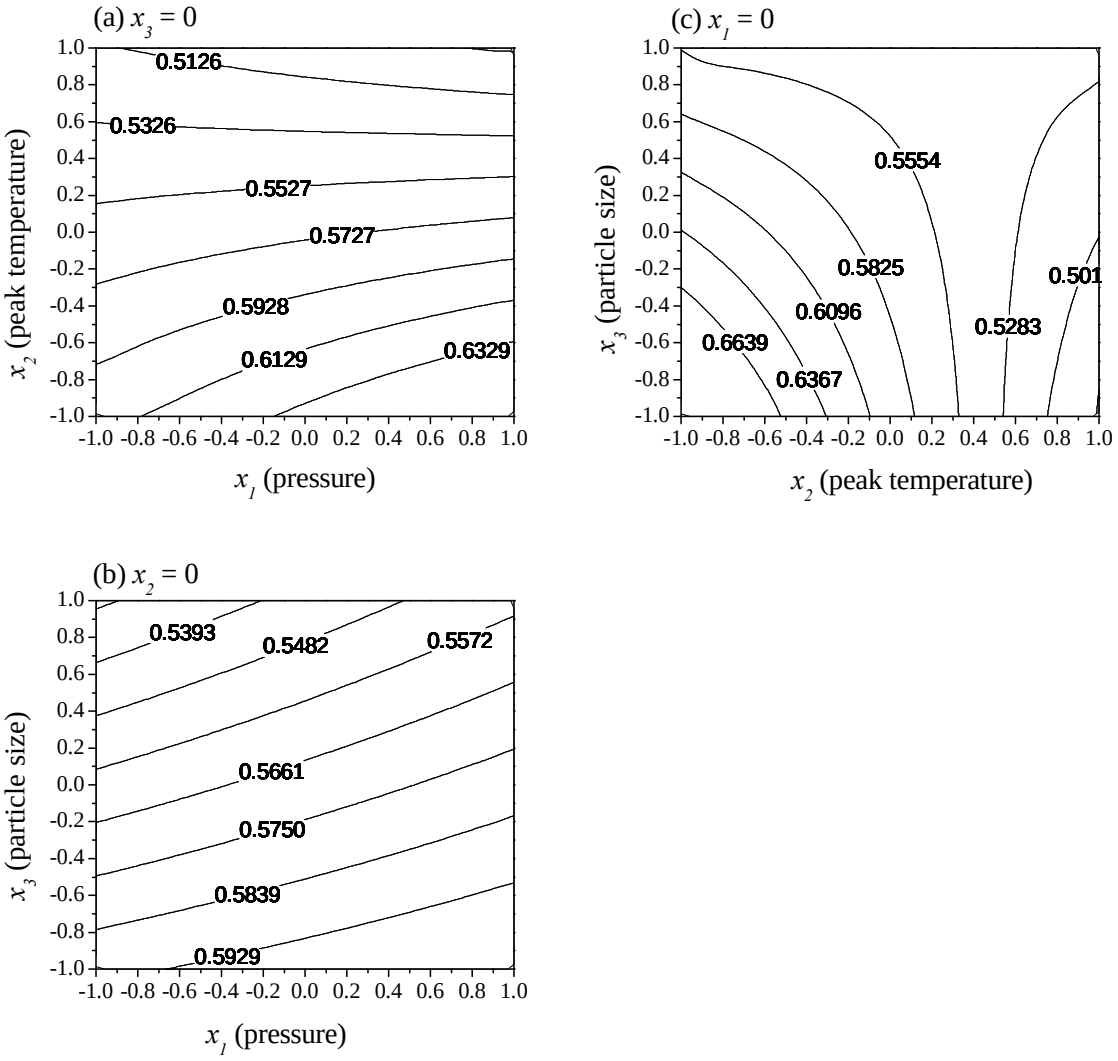

Fig. 2. Contour plots showing the effects on the biochar yield (y_{char}) of (a) pressure and peak temperature, (b) pressure and particle size, and (c) peak temperature and particle size.

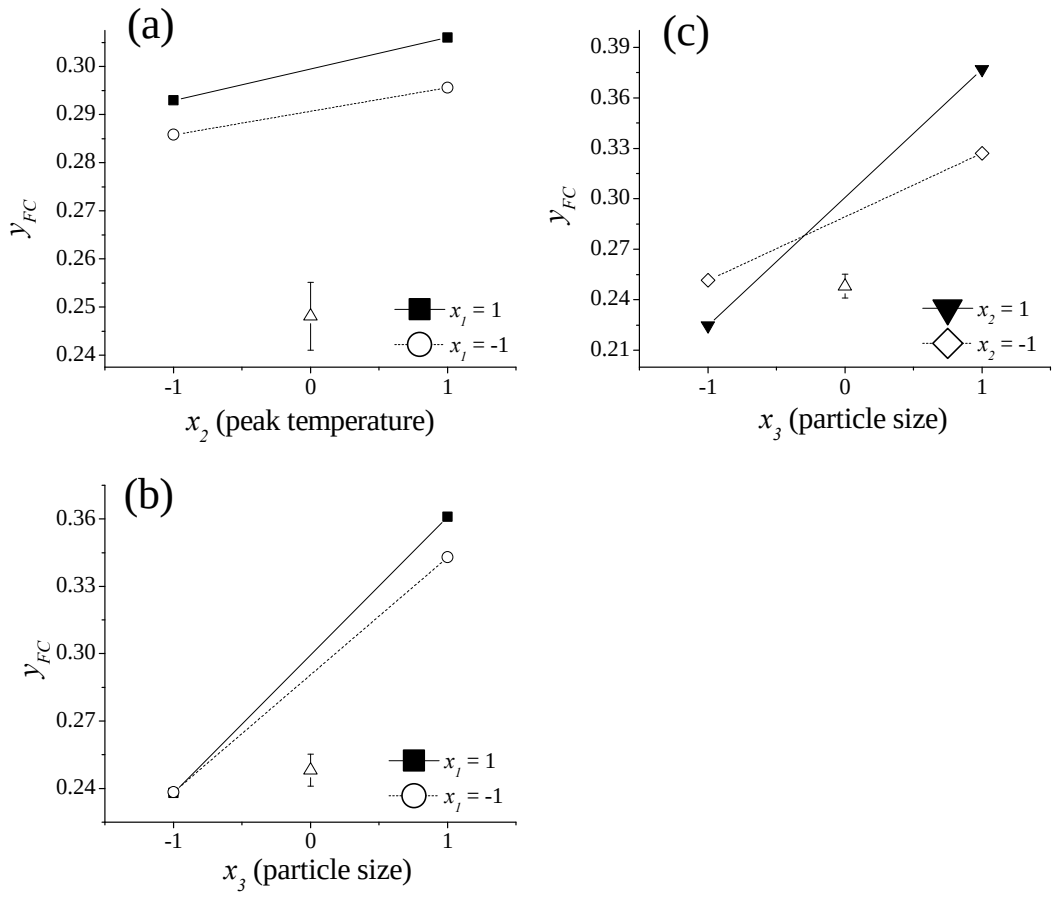

Fig. 3. 2-factor interaction effect plots for the fixed-carbon yield (y_{FC}): (a) pressure and peak temperature (x_3 =0), (b) pressure and particle size (x_2 = 0), and (c) peak temperature and particle size (x_1 = 0).

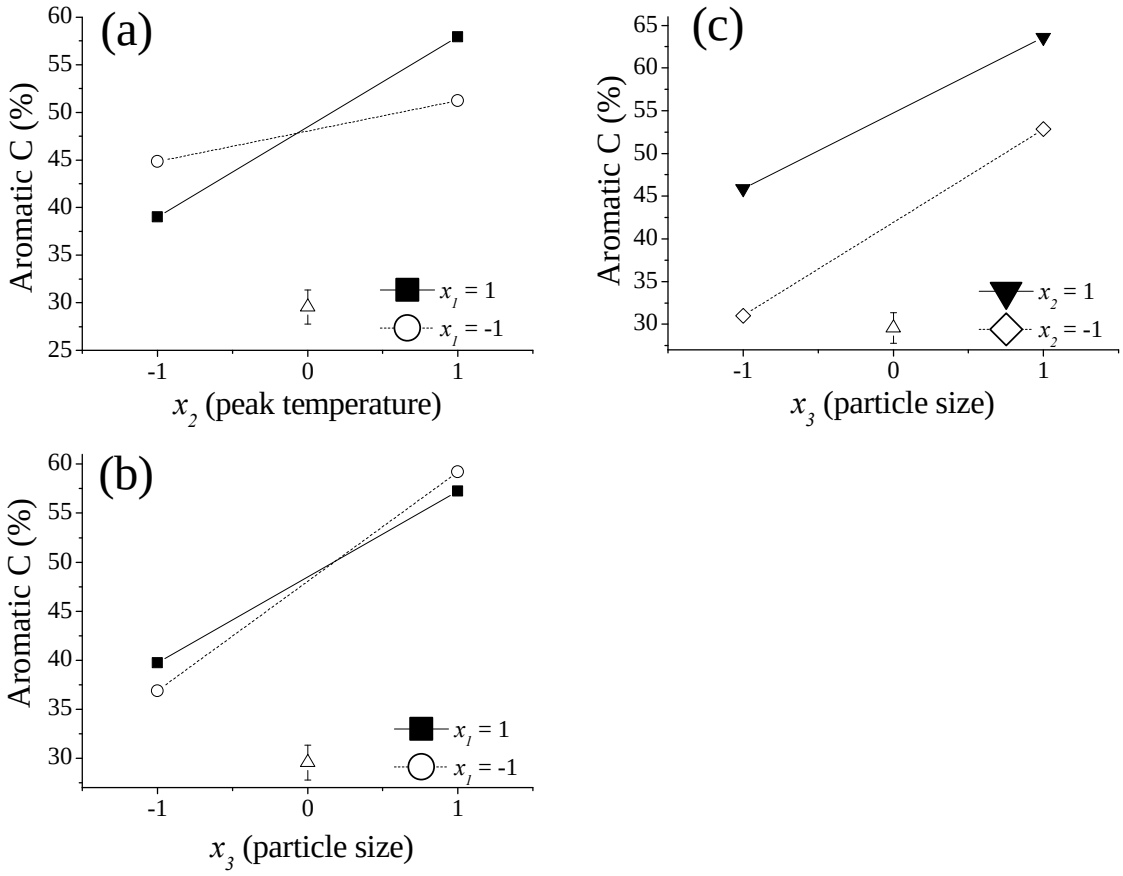

Fig. 4. 2-factor interaction effect plots for the percentage of aromatic C: (a) pressure and peak temperature (x_3 =0), (b) pressure and particle size (x_2 = 0), and (c) peak temperature and particle size (x_1 = 0).

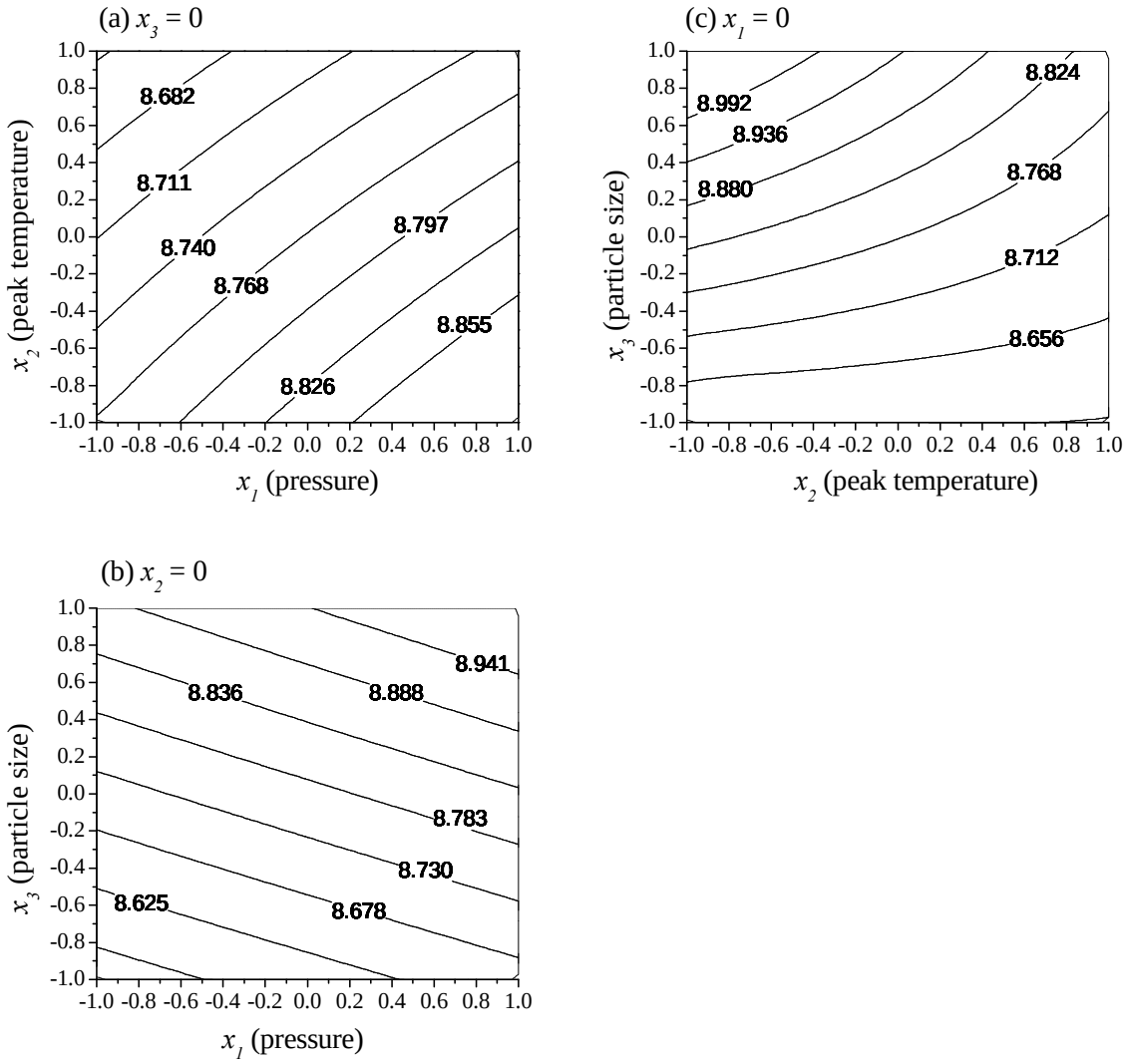

Fig. 5. Contour plots showing the effects on the *pH* of (a) pressure and peak temperature, (b) pressure and particle size, and (c) peak temperature and particle size.